Seismic Traveltime Analysis for Some Stations around Parkfield, California

Abel U. Osagie, School of Physics, Universiti Sains Malaysia, Pulau Penang 11800, Malaysia

*Adepelumi, A.A, Department of Geology, Obafemi Awolowo University, Ile-Ife, Nigeria.

Falade, A.H, Department of Geology, Obafemi Awolowo University, Ile-Ife, Nigeria.

*Corresponding author's: Email: (aadepelu@oauife.edu.ng)

Abstract

Digital seismic records of Northern California Seismic Network (NCSN) covering a period of three years (from 1st January, 2010 to 31st December, 2012) have been used to investigate the average traveltime residuals of some seismic stations in the vicinity of Parkfield. During this period, 199 stations records of 61315 P-wave arrival-time picks, and 6366 S-wave arrival-time picks from a total of 1911 events were used for this study. Synthetic traveltimes were generated using the United State Geological Survey (USGS)1-D P-wave velocity model that incorporates a customized two-point ray tracing algorithm. The velocity model obtained suggests that refracted waves are likely the first-arrival phases at most of the Parkfield seismic stations. Comparison between the recorded data set and the synthetic traveltimes show that more than 99% of the P-wave arrival times recorded by each station have traveltime residual values between -2s and +2s. The comparison also show positive average residual values between 0.11s and 0.75s for some stations which include: BMS, PAR, PDR, PJC and WRD. However, most of the stations show negative average residuals that range from -1.28s for station BCW to -0.05s for station B900.It is deduced that the computed average residuals can reduce errors attributable to station correction in the inversion of hypocentral parameters in the vicinity of the study region.

Keywords: Stations, Parkfield, P-waves, Traveltime, Residuals

1. INTRODUCTION

In addition to limitations imposed by data quality, station distribution, the algorithm and velocity model used to predict data, appropriate traveltime corrections for seismic stations is desired for reliable determination of hypocentral parameters. Waldhauser and Schaff, (2008) attributed hypocenter location uncertainties to inaccuracies in the phase picks and errors in the model used to predict the data. Even with accurate phase picks, and reliable model, station correction plays a significant role in the hypocentral parameters inversion process. In a region like Parkfield that is reported to have different basement rocks juxtaposed by the San Andreas Fault (SAF) system, a single traveltime residual value for a station may not be suitable to every hypocentral parameters inversions. However, from record of many events, an average value of traveltime residual obtained from generating synthetic traveltimes for a seismic station using a reliable velocity model can reduce location uncertainties caused by the use of inaccurate station corrections.

Three years seismic records of Northern California Seismic Network (NCSN) were used to investigate the average traveltime residual of some seismic stations around Parkfield, California. Over 96% of the recorded seismic events show relatively small number of S-wave picks; thus, only P-wave picks were employed for the analysis. More than Ninety seismic stations recorded an average of 100 events during the period under investigation. Generally, during this period, a total of 1911 events were recorded.

It has been shown by various authors that a number of forward modeling technique are available for the generation of synthetic travel times. However, the choice of the method to be adopted generally depends on a tradeoff between the accuracy necessary, and the desired computing time. The complexity of the model and geology of the region where the data were acquired, on one hand, and the noise level and uncertainty associated with the data usually dictate the method that should be used. One-dimensional models cannot predict travel times accurately for local and regional distances (*Kennett and Engdahl, 1991, Kennett et al., 1995*). The computation of travel times in heterogeneous media is a complicated problem (Cerveny, 2001)

Two classes of seismic modeling, that is, the ray tracing (Zhao et al. 2006; Cerveny and Psencik,1984 and wave equation (Tong et al. 2014) methods are routinely implemented for numerical forward modeling of seismic waves. Both classes exists for one, two, and three dimensions, For the purpose of this study, the modified version of the two dimensional ray tracing techniques developed by Kim and Baag (2002) was adopted because of its flexibility, accurate traveltimes estimation and reduced computation time,

2. GEOLOGY AND VELOCITY MODEL

The region of interest lies within Latitude N35º-N37ºand longitude W120º-W122º. Spanning over 40000 square kilometers. The study area covers the transition between the creeping segment of San Andreas Fault (SAF) to the northwest and the locked segment to the southeast. The geology of Parkfield region is dominated by the SAF system and has three other faults which are believed to play varying roles in the local geology ([Sims, 1990; Sims and Hamilton, 1990). The stratigraphy of the area revealed that Salinian granitic rocks are the basement rocks. This is covered by a maximum of 2 km of Tertiary and Quaternary marine and non-marine sediments; and volcanics rocks on the southwest side of the fault, and Franciscan rocks and Great Valley sequence on the northeast side (Walter and Mooney, 1982; Lees and Malin, 1990). Velocity models there show high V_p/V_s ratio along the fault near the surface and at depth within the fault zone, and a pronounced strong vertical velocity gradient in the upper 2 km of the section (Michelini and McEvilly, 1991; Eberhart-Phillips and Michael, 1993).

The United State Geological Survey (USGS) P-wave velocity model for Parkfield region is shown in table 1. The model is composed of nine layers with irregular intervals between boundaries consisting of a 0.25 km-thick top layer with a relatively low P- and S-wave velocity and a high velocity contrast across the second and the third boundaries. This is represented in Figure 1.

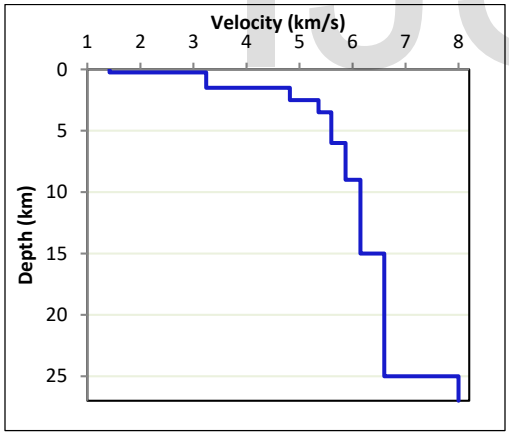

Table 1 The USGS Parkfield model

Layer	Depth (Km)	Velocity (Km/s)
1	0.00	1.42
2	0.25	3.24
3	1.50	4.82
4	2.50	5.36
5	3.50	5.60
6	6.00	5.87
7	9.00	6.15
8	15.00	6.60
9	25.00	8.00

Figure 1: Velocity Depth function

Station and Events Distribution

We observed that, over 200 stations recorded one or more events between 1st January, 2010 and 31st December, 2012. 92 stations with record of 100 or more P-wave arrival-time picks were selected for this study. The stations are distributed within latitude N35º 19′ - N36º 45′ and

longitude W120º00′ - W121º46′ (Figure 2).Many of the selected stations recorded more than 1000 P-wave arrivals.

From NCSN catalog, a total of 1911 events were recorded during the period. The events are clustered within latitude N35º 33′–N36º 18′ and longitudeW120º05′–W120º54′ as shown in Figure 3. The cluster covers the creeping central segment of the San Andreas Fault (SAF) northwest of Middle Mountain. The SAF slip in the region is not accommodated along a single fault line, but rather along individual sub-parallel active stands (Waldhauser et. al, 2004).

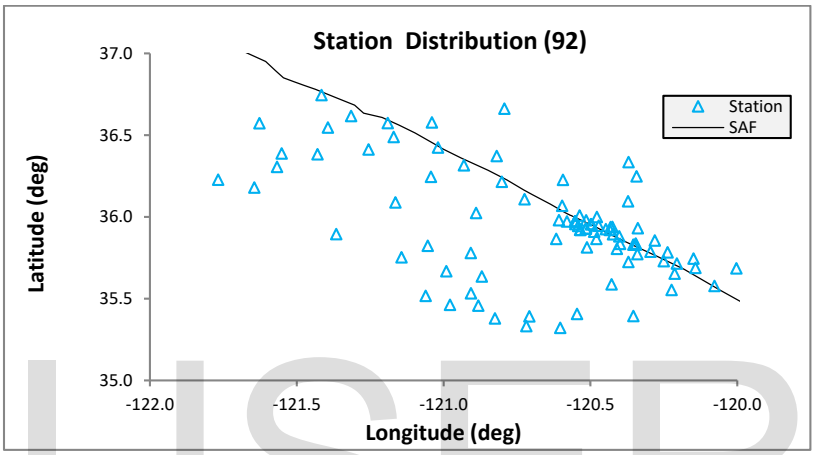

Figure 2: Station distribution and the San Andreas Fault (SAF) line

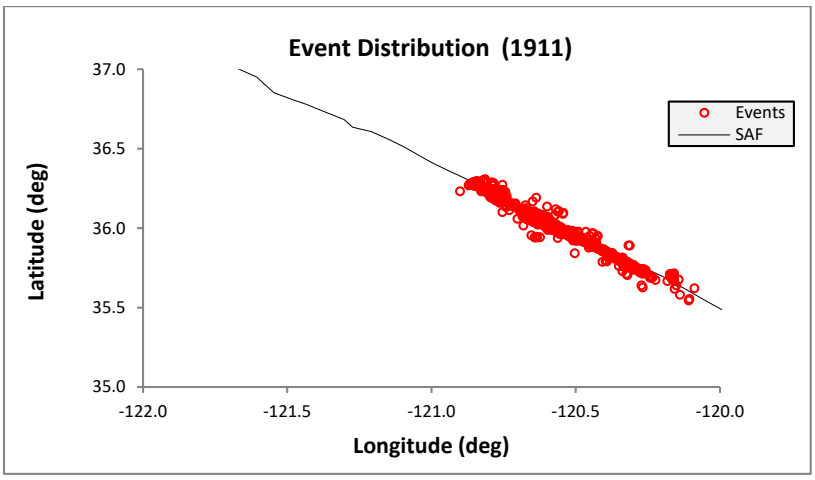

Figure 3: Event distribution and the San Andreas Fault (SAF) line

3. VELOCITY MODEL ANALYSIS

The model has high velocity contrast between the first three layers. The velocity contrast is highest between the first and second layers (1.82 km/s). This suggests that for events of shallow depths (0-1 km), refracted waves from multiple boundaries are first-arrival phases to most recording stations within the region. First-arrival phases may also be dominated by refracted waves at focal depths of 1-4 km. Ray paths are computed for refracted waves off the bottom of a few boundaries beneath the source layer. Figure 4(a) shows the ray paths of refracted wave from the bottom of the first four boundaries beneath the source layer (focal depth of 1 km), and from the 25 km boundary. Figure 4(b) is another example of ray paths at 3 km focal depth. Figure 4 also show three more ray paths at equal intervals for the refracted waves.

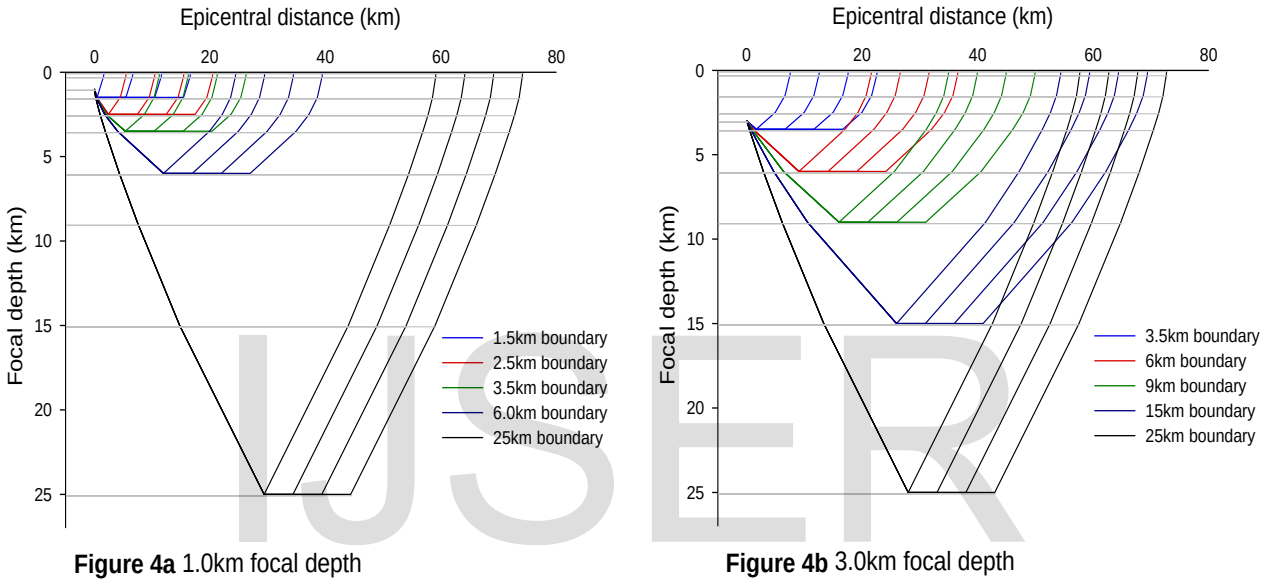

Figure 4a 1.0km focal depth **Figure 4b** 3.0km focal depth

Figure 4 Ray paths of refracted waves from some boundaries beneath the source layer for (a) 1km and (b) 3km.

Using the velocity model, cross-over distances at some selected depths for coincident epicenter were also computed. It is observed, that for the first few layers, refracted waves dominated first-arrivals at the seismic stations. Figures 5(a)-(f) show travel-time curves at some selected depths. For shallow events (depths ≤ 1.0km), only stations with less than 2 km epicentral distance record direct wave as first arrivals. As the station epicentral distance increases, first-arrivals progressively become waves refracted off the bottom of: the source layer, first layer beneath the source layer, second or even third layer beneath the source layer, in that order. At a focal depth of 1km (Fig. 5a), most stations record first-arrivals as waves refracted off the 3.5 km and 6 km boundaries. Waves refracted off the 25 km-boundary become first-arrivals beyond 90km epicentral distances. At 3 km focal depth (Fig. 5b) first-arrivals are direct waves for epicentral distances less than 8 km. However, first-arrivals are dominated by refracted waves beyond 8 km epicentral distances. Apparently, for focal depths less than 5 km, first-arrivals appear to be refracted waves from either the bottom of the source layer or from the bottom of the first and

even second layers beneath the source layer. The model suggest that only at focal depths greater than 7 km that most stations of epicentral distances less than 80 km record direct wave as first-arrivals as depicted in Figures 5(e) and 5(f) respectively. Based on this geologic model and the derived travel times ray paths, it is evident that, earthquake relocation in the study region will depend mostly on refracted waves rather than direct waves. The refracted waves show more sensitivity to difference in velocity structure between the true and used models (Osagie and Kim, 2013) and therefore, have the tendency to increase errors in determination of hypocentral parameters in the region.

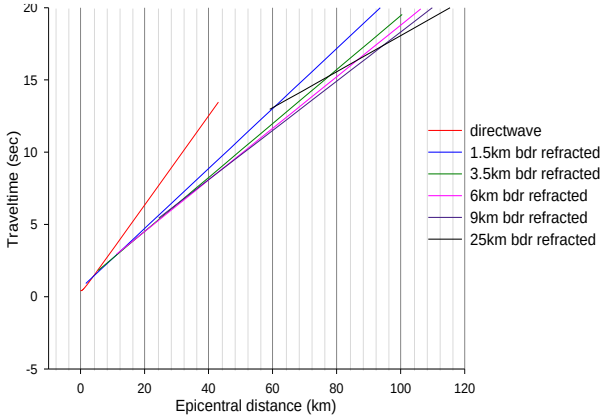

Figure 5a Focal deoth of 1.0km

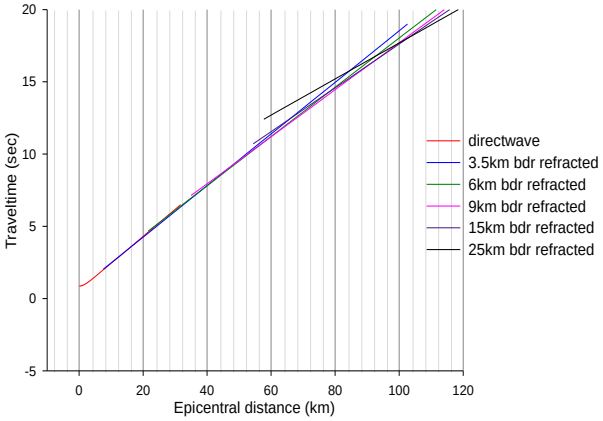

Figure 5b Focal deoth of 3.0km

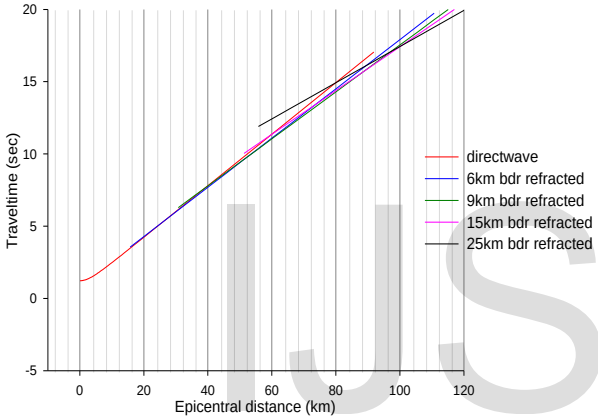

Figure 5c Focal deoth of 5.0km

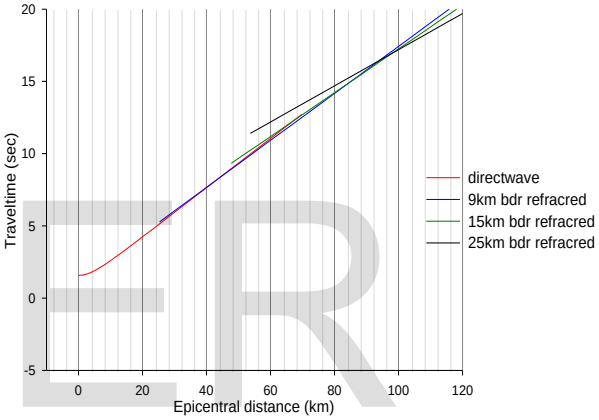

Figure 5d Focal deoth of 7.0km

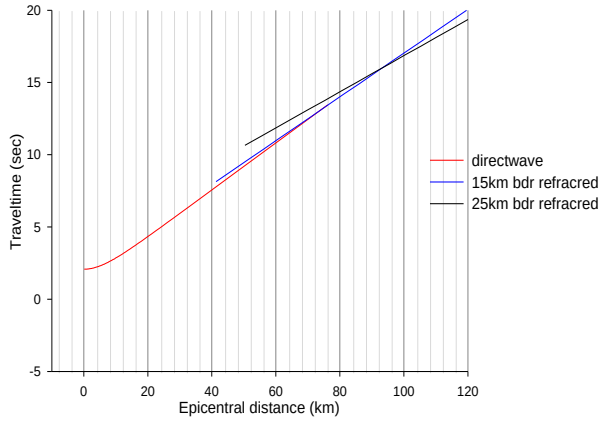

Figure 5e Focal deoth of 10km

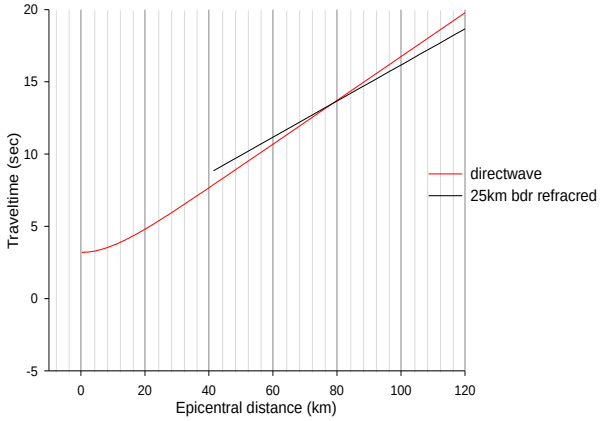

Figure 5f Focal deoth of 17km

Figure 5 Distance-travel time curve for directwaves (red line),refraction off other boundaries at focal depths of (a)1km, (b)3km, (c) 5km, (d) 7km, (e) 10km and (f) 17km.

4. TRAVELTIMES COMPARISON OE THE MODEL

Hypocentral parameters of 1911 events from the digital seismic records of NCSN over the three-year period was used to generate synthetic traveltime of first-arrival *P* phase at the selected 92 stations. An adapted version of *ncsn2pha* (Fred, 2001) was used to convert Hypoinverse Y2000 record phase format into the required phase format. The traveltime data were synthesized using a modified version of a two-point ray tracing algorithm (Kim & Baag, 2002) and the USGS velocity model for Parkfield region. The calculated traveltimes were compared with the reported traveltimes for each event and for each station. The differences between the calculated and reported traveltimes were mostly within the interval of ±2 seconds as shown in table 2. For each station in the table 2, columns 2, 3, 4 and 5 represent; station code, latitude, longitude and elevation respectively. Columns 6-11 are defined below.

Column 6 number of positive differences between calculated and the reported traveltimes
Column 7 number of negative differences between calculated and the reported traveltimes
Column 8 number of P wave arrival-time picks used
Column 9 number of P wave arrival-time picks reported
Column 10 difference between the reported and used arrival-time picks
Column 11 percentage ratio between the used and reported arrival-time picks

Figures 6(a)-(c) show the spread between the calculated and reported traveltimes for some stations. Figure 6(a) shows five stations with positive average values, while figure 6(b) distinctively revealed five stations with the largest negative average values. Figure 6(c) shows four stations with larger number of P wave arrival-picks and varying negative average values.

5. CONCLUSION

Ninety two stations in the vicinity of Parkfield recorded a total of 58382P-wave arrival-time picks in three years. When compared with the reported traveltime for the same velocity model, synthetic traveltime differences varied between -2s and +2s for all the stations investigated. Positive average time residual values with range between 0.11s and 0.75s was deduced for five stations which include; BMS, PAR, PDR, PJC and WRD. The comparisons also show negative average residual values ranging from -1.28s for station BCW to -0.05s for station B900. We deduced that the computed average residuals can reduce errors attributable to station correction in the inversion of hypocentral parameters in the vicinity of the study region. Based on the presented model results derived using 2D ray tracing technique, it can be concluded that this method is a useful and efficient tool for the estimation of travel times ray paths and the computation of the travel residual times of both local and teleseismic events.

Table 2 The Selected 92 station coordinates and their calculated residual values

	STN	Latitude (deg)	Longitude (deg)	Elev (km)	Res (+ve)	Res (-ve)	No. Used	No. Reptd	Diff	Used (%)	Ave Res
1	ARD	35.4632	-120.9783	0.091	16	87	103	103	0	100	-0.12
2	B072	35.8310	-120.3450	0.397	6	851	857	859	2	99.77	-0.44
3	B073	35.9467	-120.4717	0.535	41	1423	1464	1467	3	99.8	-0.27
4	B075	35.9292	-120.5153	0.583	11	1154	1165	1169	4	99.66	-0.64
5	B076	35.9398	-120.4248	0.445	298	1210	1508	1515	7	99.54	-0.15
6	B078	35.8377	-120.3452	0.387	4	838	842	844	2	99.76	-0.41
7	B079	35.7157	-120.2057	0.437	3	457	460	460	0	100	-0.4
8	B900	35.6860	-120.0030	0.219	66	191	257	258	1	99.61	-0.05
9	B901	35.6897	-120.1420	0.275	21	342	363	364	1	99.73	-0.25
10	BAP	36.1804	-121.6444	1.193	0	143	143	145	2	98.62	-1.13
11	BBGB	36.5785	-121.0396	1.089	18	179	197	201	4	98.01	-0.18
12	BCW	36.3065	-121.5669	1.505	2	92	94	106	12	88.68	-1.28
13	BJC	36.5472	-121.3939	0.173	28	239	267	267	0	100	-0.52
14	BJOB	36.6181	-121.3147	1.052	0	111	111	111	0	100	-1.17
15	BL	35.5338	-120.9067	0.457	1	194	195	195	0	100	-0.48
16	BMS	36.6631	-120.7929	0.78	100	11	111	112	1	99.11	0.24
17	BP	35.7537	-121.1432	0.792	0	188	188	188	0	100	-0.65
18	BPC	36.5734	-121.6269	0.173	63	81	144	144	0	100	-0.1
19	BPI	36.4901	-121.1696	0.301	5	158	163	164	1	99.39	-0.7
20	BPO	36.2284	-121.7677	0.33	3	106	109	109	0	100	-0.55
21	BRV	36.4247	-121.0191	0.525	28	225	253	254	1	99.61	-0.17
22	BSG	36.4138	-121.2552	0.161	1	229	230	236	6	97.46	-0.78
23	BSM	36.3837	-121.4292	0.884	0	120	120	121	1	99.17	-1.02
24	BVL	36.5749	-121.1901	0.479	16	141	157	160	3	98.12	-0.45
25	BVY	36.7462	-121.4158	0.647	8	98	106	106	0	100	-0.65
26	CCRB	35.9572	-120.5516	0.595	10	1610	1620	1629	9	99.45	-0.63
27	EADB	35.8952	-120.4226	0.469	81	1234	1315	1316	1	99.92	-0.33
28	EC	35.3333	-120.7182	0.259	3	116	119	119	0	100	-0.35
29	FROB	35.9109	-120.4869	0.515	17	1281	1298	1302	4	99.69	-0.61
30	GHIB	35.8323	-120.3473	0.393	4	782	786	788	2	99.75	-0.44
31	HAST	36.3887	-121.5514	0.542	0	192	192	192	0	100	-0.88
32	JCNB	35.9390	-120.4311	0.533	190	374	564	568	4	99.3	-0.05
33	JCSB	35.9212	-120.4340	0.454	338	1103	1441	1446	5	99.65	-0.12
34	LCCB	35.9800	-120.5142	0.385	151	1394	1545	1554	9	99.42	-0.2
35	LMD	35.3803	-120.8247	0.171	4	137	141	141	0	100	-0.33
36	LQ	35.6688	-120.9907	0.619	1	145	146	146	0	100	-0.48
37	MH022	35.9742	-120.5521	0.66	3	173	176	177	1	99.44	-0.95
38	MH023	35.9742	-120.5521	0.66	0	423	423	423	0	100	-0.97
39	MH025	35.9742	-120.5521	0.66	3	555	558	562	4	99.29	-0.98
40	ML	35.3225	-120.6025	0.762	2	122	124	124	0	100	-0.61
41	MMNB	35.9565	-120.4960	0.701	28	1469	1497	1501	4	99.73	-0.32
42	PAGB	35.7306	-120.2499	0.48	3	474	477	479	2	99.58	-0.38
43	PAN	35.7801	-120.9071	0.426	1	246	247	249	2	99.2	-0.43
44	PAP	35.8958	-121.3655	1.044	1	190	191	191	0	100	-1.15
45	PAR	36.2493	-120.3428	0.452	117	9	126	127	1	99.21	0.67
46	PBM	35.3944	-120.3539	1.049	0	162	162	163	1	99.39	-1.12
47	PBP	35.5791	-120.0775	0.569	43	159	202	202	0	100	-0.12
48	PBS	35.7457	-120.1490	0.811	7	355	362	362	0	100	-0.54
49	PBW	36.3167	-120.9309	0.302	3	358	361	362	1	99.72	-0.41
50	PCA	35.9315	-120.3383	1.163	261	465	726	728	2	99.73	-0.08

Table 2 The Selected 92 station coordinates and their calculated residual values

	STN	Latitude (deg)	Longitude (deg)	Elev (km)	Res (+ve)	Res (-ve)	No. Used	No. Reptd	Diff	Used (%)	Ave Res
51	PCB	35.5184	-121.0607	0.164	7	93	100	100	0	100	-0.14
52	PCC	36.0898	-121.1636	0.372	8	698	706	715	9	98.74	-0.42
53	PCM	35.8055	-120.4096	0.671	5	875	880	882	2	99.77	-0.33
54	PDR	36.3358	-120.3700	0.428	170	1	171	172	1	99.42	0.75
55	PGH	35.8308	-120.3538	0.405	8	560	568	569	1	99.82	-0.42
56	PHA	35.8362	-120.3986	0.398	6	750	756	757	1	99.87	-0.29
57	PHF	35.8816	-120.4016	0.457	57	648	705	706	1	99.86	-0.25
58	PHL	35.4077	-120.5456	0.355	5	160	165	166	1	99.4	-0.74
59	PHOB	35.8666	-120.4796	0.796	4	918	922	923	1	99.89	-0.53
60	PHP	35.9805	-120.6068	0.548	9	1689	1698	1707	9	99.47	-0.54
61	PHR	36.3730	-120.8189	0.707	16	299	315	316	1	99.68	-0.3
62	PHSB	35.8240	-121.0539	0.475	0	418	418	420	2	99.52	-0.59
63	PIR	35.5544	-120.2233	0.471	14	304	318	318	0	100	-0.26
64	PJC	36.0959	-120.3716	0.403	496	11	507	509	2	99.61	0.6
65	PJU	36.2270	-120.5935	0.925	280	380	660	660	0	100	-0.1
66	PKD	35.9452	-120.5416	0.583	13	1681	1694	1705	11	99.35	-0.59
67	PKL	35.7730	-120.3399	0.422	8	679	687	689	2	99.71	-0.28
68	PL11B	35.9745	-120.5516	0.659	5	977	982	984	2	99.8	-0.57
69	PLO	36.2463	-121.0430	0.251	6	557	563	565	2	99.65	-0.56
70	PMC	35.7252	-120.3706	0.471	2	384	386	388	2	99.48	-0.24
71	PMM	35.9563	-120.4985	0.751	38	1140	1178	1178	0	100	-0.24
72	PMPB	36.2159	-120.8013	0.802	24	728	752	757	5	99.34	-0.55
73	PMR	35.7843	-120.2368	0.498	17	369	386	386	0	100	-0.32
74	PPO	35.8667	-120.6160	0.446	228	1331	1559	1574	15	99.05	-0.07
75	PPT	36.1091	-120.7242	0.481	15	1008	1023	1024	1	99.9	-0.4
76	PSA	36.0247	-120.8892	0.15	21	740	761	768	7	99.09	-0.31
77	PSC	35.5884	-120.4279	0.326	1	287	288	289	1	99.65	-0.35
78	PSM	36.0688	-120.5962	0.957	25	1312	1337	1342	5	99.63	-0.41
79	PSN	35.7878	-120.2951	0.39	5	536	541	543	2	99.63	-0.34
80	PSR	35.8562	-120.2804	0.48	21	815	836	837	1	99.88	-0.28
81	PST	35.9307	-120.5148	0.559	15	1344	1359	1362	3	99.78	-0.53
82	PTA	35.3925	-120.7078	0.802	5	119	124	124	0	100	-0.68
83	PTR	35.6542	-120.2133	0.594	1	213	214	214	0	100	-0.48
84	PVC	35.9221	-120.5350	0.77	16	1566	1582	1589	7	99.56	-0.61
85	PWK	35.8145	-120.5119	0.47	15	1176	1191	1196	5	99.58	-0.19
86	RAMR	35.6360	-120.8698	0.414	2	306	308	310	2	99.35	-0.47
87	RMNB	36.0009	-120.4777	1.164	27	696	723	725	2	99.72	-0.45
88	SCYB	36.0094	-120.5366	0.947	9	1398	1407	1411	4	99.72	-0.52
89	SMNB	35.9730	-120.5799	0.698	5	1462	1467	1476	9	99.39	-0.76
90	VARB	35.9261	-120.4471	0.475	115	1429	1544	1546	2	99.87	-0.19
91	VCAB	35.9216	-120.5339	0.755	15	1801	1816	1821	5	99.73	-0.78
92	WRD	35.4588	-120.8817	0.238	131	19	150	150	0	100	0.11

*Res(+ve): positive differences between used and reported, Res(-ve): negative differences between used and calculated, No.Used: number used, No Reptd: number reported, Diff: difference between used and reported, Used(%): percentage ratio between used and reported, Ave Res: average value of differences between calculated and reported traveltimes.

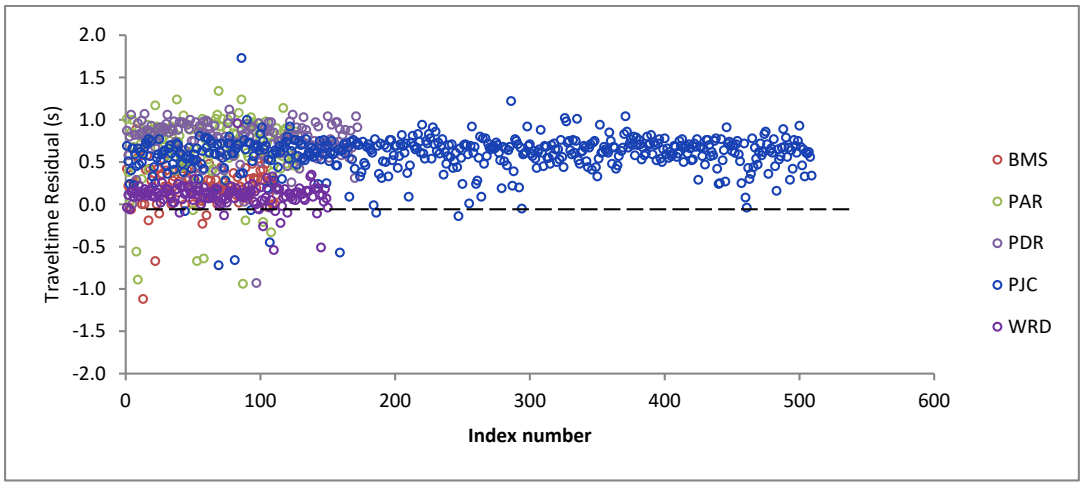

Figure 6(a) Stations with positive average residual values

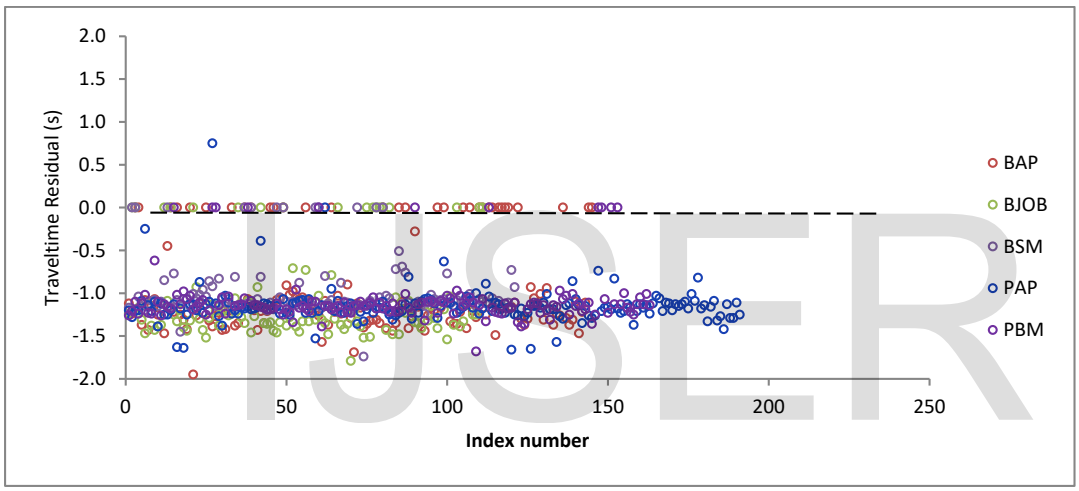

Figure 6(b)Some stations with largest negative average residual values

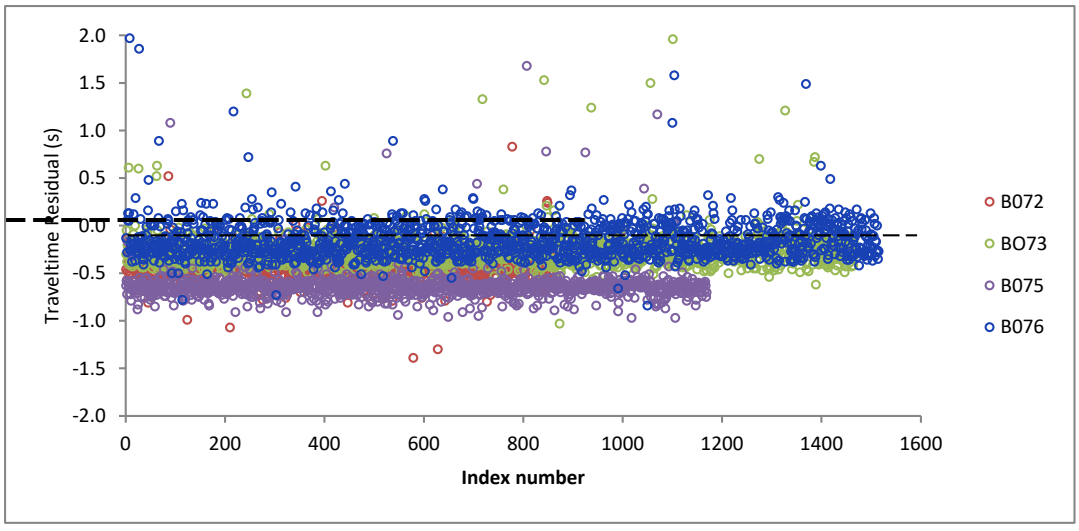

Figure 6(c)Some stations with varying negative average residual values

Acknowledgements

We thank NCSN for access to their data available at: http://quake.geo.berkeley.edu/ncsn/, Prof. Woohan Kim of Earth and Environmental Sciences, Gyeongsang National University, South Korea, through whom the data was received, and who provided the original algorithm which was modified for use in this work. This study was self-funded.

References

Cerveny, V (2001) *Seismic ray theory*, Cambridge University Press, 713 pp.

Cerveny, V and Psencik (1984) Numerical modeling of seismic wave fields in 2-D laterally varying layered structures by the ray method. In *Documentation of earthquake algorithms, Report SE-35*, E.R. Engdahl (editor), pp. 36-40, Boulder: World Data Center A for Solid Earth Geophysics.

Eberhart-Phillips, D., and A.J. Michael(1993), Three-dimensional velocity structure,seismicity, and fault structure in the Parkfield region, centralCalifornia, *J.Geophys. Res.,98*, 15737–15758.

Hahm, I.K.,W. Kim, J.M.Lee andJ.S.Jeon(2007),Determination of hypocentral parametersof local earthquakes using weighting factor based on take-off angle, (MHYPO), *Geosciences Journal,11*, 39-49.

Kennett, B.L.N., and E.R. Engdahl, (1991). Travel times for global earthquake location and phase identification. *Geophys. J. Int.*, **105,** 429-465.

Kennett, B.L.N., E.R. Engdahl, and R. Buland, (1995). Constraints on seismic velocities in the Earth from travel times. *Geophys. J. Int.,* **122,** 108-124.

Klein, F.W.(1978),Hypocenter location program HYPOINVERSE, *U.S Geol.Surv. Open File Rep.,78-694*, 113pp.

Klein, F. W.(2002),User's guide to HYPOINVERSE-2000, a Fortran program to solve for earthquake locations and magnitudes, *U.S Geol.Surv. Open FileRep,02-171*,123pp.

Kim, W. and C. E.Baag(2002),Rapid and accurate two-point ray tracing based on a quadratic equation of takeoff angle in layer media with constant or linearly varying velocity functions, *Bull.Seismol. Soc. Am., 92*, 2251-2263.

Kim, W., Hahm, I. K., Ahn, S.J., and D.H.Lim (2006), Determining the hypocentral parameters for local earthquakes in 1-D using genetic algorithms. *Geophysical Journal International, 166*, 590-600.

Kissling,E., Ellsworth, W.L., Eberhart-Phillips, D., andU.Kradolfer(1994),HYPOSAT Initialreference models in local earthquake tomography, *Journal of Geophysical Research, 99*, 19635-19646.

Li, Y.-G., W. L. Ellsworth, C. H. Thurber, P. E. Malinand K. Aki(1997),Fault-zone guided waves from explosions in the San Andreas fault atParkfield and Cienega alley,California, *Bull.Seismol. Soc. Am., 87*,210-221.

Lees,J.M and P.E.Malin(1990),Tomographic imagies of P wave velocity variation at Parkfiels, California, *Journal of Geophysical Research, 95*, 21713-21804.

Lomnitz, C.(2006),theorems of earthquake location, *Bull.Seismol. Soc. Am., 96*,306-312.

Michelini, A., and T. V. McEvilly(1991), Seismological studies at Parkfield:I. simultaneous inversion for velocity structure and hypocenter susing B-splines parameterization, *Bull.Seismol. Soc. Am., 81*,524-552

Osagie, A. U. and W. Kim (2013),Relocation of Earthquakes that Occurred Beneath Parkfield Region of California using VELHYPO, *IOSR J. Applied Geol. and Geophy., 1*, 66-81

Sieh, K. E.(1978),Slip along the San Andreas Fault associated with the great 1857 earthquake, *Bull.Seismol. Soc. Am., 68,* 1421–1448.

Sims, J.D.(1990),Geology map of the San Andreas fault zone in the Parkfield 7.5 minute quadrangle, Monterey and Fresno Counties, California, *U.S Geol.Surv. Misc. Field Stud. Map, MF-2015.*

Sims, J.D., and J. C. Hamilton(1990),Geology map of the San Andreas fault zone in the Cholame quadrangle, San Luis Obispo County, California, *U.S Geol.Surv. Misc. Field Stud. Map, MF-XXXX, in press.*

Thurber, C.H.(1992),Hypocenter-velocity structure coupling in local earthquaketomography,*Physics of the Earth and Planetary Interiors, 75,* 55-62.

Tong, P., Zhao, D., Yang, D., Yang, X., Chen, J and Liu, Q (2014) Wave-equation based traveltime seismic tomography – Part 1: Method. Solid Earth Discuss. 6, 2523–2565.Waldhauser, F. and D.P.Schaff(2008),Large-scale relocation of two decades of northern Californiaseismicity using cross-correlation and double-difference methods,*J.Geophys. Res.,113*, B08311, doi:10.1029/2007JB005479.

Waldhauser, F., W.L. Ellsworth, Schaff, D.P., and A.Cole (2004), Streaks, multiplets, andholes: High-resolution spatio-temporal behavior of Parkfield seismicity, *Geophys. Res.Lett., 31*, L18608, dol 10.1029/2004GL020649.

Waldhauser, F., andW.L. Ellsworth(2000),A double-difference earthquakelocationalgorithm: method and application to the Northern Hayward fault, California, *Bull.Seismol. Soc. Am., 90,* 1353-1368.

Walter, A.W. and W. D.Mooney (1982), Crustal Structure of the Diablo and Gabilan ranges, Central California: a reinterpretation of existing data, *Bull.Seismol. Soc. Am.,72*, 1567-1590.

Zhao, A. H., Zhang, M. G and Ding Z.F (2006) Travel time computation for traversely isotropic media. Chinese Journal of Geophysics. Vol, 49 (6) pp. 1603-1612.